Influence of electromagnetic fields on the dielectronic recombination of Ne^{7+} ions

S. Böhm, S. Schippers, W. Shi, and A. Müller
Institut für Kernphysik, Universität Giessen, 35392 Giessen, Germany

N. Djurić, G. H. Dunn, and W. Zong
JILA, University of Colorado and NIST, Boulder, Colorado 80309-0440

B. Jelenković
Institute of Physics, Pregrevica 118, 10800 Belgrade, Yugoslavia

H. Danared
Manne Siegbahn Laboratory, 10405 Stockholm, Sweden

N. Eklöw, P. Glans, and R. Schuch
Atomic Physics, Stockholm University, 10405 Stockholm, Sweden
(Received 16 March 2001; published 13 August 2001)

The influence of crossed electric and magnetic fields on dielectronic recombination of Ne^{7+} ions has been measured at the Stockholm heavy-ion storage ring CRYRING. The electron energy range covered all dielectronic recombination resonances attached to $2s \rightarrow 2p_{1/2}$ and $2s \rightarrow 2p_{3/2}$ $\Delta n = 0$ core excitations. Two sets of measurements at magnetic fields of 180 mT and 30 mT have been performed. For the measurement at 180 mT we applied 25 different electric fields between 0 and 1400 V/cm. The resonance strength for dielectronic recombination via high Rydberg states initially increases linearly with electric field and later levels out. At a magnetic field of 30 mT we applied 15 different electric fields ranging from 0 to 140 V/cm. Compared to the measurement at 180 mT the initial slope of the rate enhancement was larger by almost a factor of 2. The fraction of resonant strength not measured due to field ionization is estimated by a model calculation of dielectronic recombination cross sections.

DOI: 10.1103/PhysRevA.64.032707 PACS number(s): 34.80.Lx

I. INTRODUCTION

Dielectronic recombination (DR) of an ion and an electron can be viewed as a two-step process in which dielectronic capture of a projectile electron into a doubly excited intermediate state is followed by radiative decay of this state to a bound level below the first ionization limit. For the present case, DR can be represented by

$$\begin{aligned} e^- + \mathrm{Ne}^{7+}(1s^2 2s_{1/2}) &\rightarrow \mathrm{Ne}^{6+}(1s^2 2p_j nl) \\ &\rightarrow \begin{cases} \mathrm{Ne}^{6+}(1s^2 2s_{1/2} nl) + h\nu & \text{(type I)} \\ \mathrm{Ne}^{6+}(1s^2 2p_j n'l') + h\nu' & \text{(type II)}, \end{cases} \end{aligned} \tag{1}$$

where $j = 1/2$ or $3/2$, and type I and type II stabilization routes are not distinguishable in our experiment. The lowest Rydberg state that is energetically allowed is at $n = 7$. As a consequence of this scheme, the final result of the recombination is susceptible to external influences on the capture stage of the system. Such influences could be collisions with other particles, interactions with a laser or even with static external electromagnetic fields [1,2]. In weak external electric fields Stark mixing of states within one nlm-Rydberg manifold occurs (with m being still a good quantum number). As the zero-field autoionization rates are rapidly decreasing with angular momentum l the mixing results in autoionization rates that are lower for low-l and higher for high-l states as compared to the field-free situation. The net effect is an increase of the number of states participating in DR, i.e., an increase of the DR cross section [3]. An additional magnetic field perpendicular to the electric field mixes the m states, which further influences the recombination rate. At low magnetic fields m-mixing typically enhances the electric field effect. At higher magnetic fields the rate decreases, because of the increasing energy splitting of the m levels, which hampers the mixing of these states [4].

The aim of the present investigation with Li-like Ne^{7+} ions is to extend a series of measurements of DR in external electromagnetic fields (DRF) on lithiumlike ions (Si^{11+} [5], Cl^{14+} [6], Ti^{19+} [7], and Ni^{25+} [8]) to elements with lower nuclear charge Z. The cross section of DR is given by

$$\sigma_{n,l} = S_0 \frac{g_d}{g_i} \frac{\pi}{E_n} \left[\frac{A_a(n,l) A_r(n,l)}{A_a(n,l) + A_r(n,l)} \right], \tag{2}$$

where A_r is the radiative rate of the intermediate resonant state $|d\rangle$ with configuration $2p_j nl$ and A_a is the autoionization rate. The quantities $g_d = 2(2j+1)(2l+1)$ and $g_i = 2$ are the statistical weights of the intermediate and initial state, respectively, E_n is the resonance energy and S_0 is a constant. Approximate values of quantities entering into Eq. (2) for Ne^{7+} are given in Table I. The radiative rates A_r strongly increase with Z. It is expected that with lower Z more n states and within a given n manifold more l states take part in DR

 ©2001 The American Physical Society

TABLE I. Parameters used for the fitting of a model spectrum based on Eqs. (2), (13), and (14) to an experimental Ne^{7+}-DR spectrum.

Model parameter	$2s\rightarrow 2p_{1/2}$	$2s\rightarrow 2p_{3/2}$
E_∞ (eV) [a]	15.93	16.10
S_0 (10^{-30} cm^2 eV^2 s) [a]	8.79	17.6
$A_r(10^8/\mathrm{s})$	5.61	5.82
$A_a^{(0)}$ (10^{14}/s) [a]	6.28	6.32
d [a]	0.32	0.61
$kT_\parallel$ (meV) [a]	0.15	0.15
$kT_\perp$ (meV) [a]	20	20
$n_{\min}$	10	10
q	7	7

[a]Varied in the fit.

and therefore the sensitivity of l mixing in an electric field increases. That means the enhancement due to an electric field should increase. On the other hand the binding energy for lower Z values decreases rapidly for given n and field ionization in the motional electric field caused by the charge state analyzing dipole magnet located behind the interaction region sets in at much lower fields (see Table II). As a consequence, states that potentially exhibit a large enhancement do not contribute to the measured DR signal. With two counteracting effects, DRF decreasing with Z and the detectability of high Rydberg states increasing with Z, the detected enhancement rate should have its maximum for a certain value of Z. In previous measurements the detected enhancement increased from Ni^{25+} ($Z=28$) to Si^{11+} ($Z=14$). One goal of this study is to clarify whether this trend persists down to $Z=10$. Another goal is the confirmation of saturation of the enhancement of the recombination rate with increasing electric field, which should occur when maximum l mixing is achieved.

II. EXPERIMENT

The experiment was performed on the heavy-ion storage-ring CRYRING at the Manne Siegbahn Laboratory in Stockholm. $^{20}Ne^{7+}$ ions were produced in the cryogenic electron beam ion source CRYSIS then preaccelerated by a radio-frequency quadrupole accelerator to about 300 keV/u and injected into the ring. After injection the storage ring was operated in the synchrotron mode to accelerate the ions to the required energy. In the present experiment we had a beam of 11.4 MeV/u $^{20}Ne^{7+}$ ions stored in the ring with intensities of up to 2 μA. The injected beam has a large longitudinal and transverse energy spread and therefore has to be cooled. This is achieved using an electron cooler (Fig. 1) installed in one section of the ring. It consists of three main parts: the electron gun, the interaction region, and the collector. Each part is surrounded by a solenoid on which correction dipole magnets are placed. Two toroid magnets are used to deflect the electron beam into and out of the interaction region. An electron beam with a diameter of 4 mm is emitted from the cathode. The electron gun is operated such that the electron current I_e is independent of the cathode voltage. The longitudinal temperature characteristic of the energy spread of the electron beam is reduced by the electrostatic acceleration of the electrons and in this experiment is given by $kT_\parallel \approx 0.13$ meV as derived by fitting a Gaussian curve to one of the resonances. Here k is the Boltzmann constant and $T_\parallel$ the longitudinal temperature. To reduce the transversal energy spread the electron beam is adiabatically expanded in a decreasing axial magnetic field [9]. The transverse temperature $T_\perp$ of the expanded beam is given by

$$\frac{kT_\perp}{B}=\frac{kT_{\perp 0}}{B_0}. \tag{3}$$

Here B_0 is the high-magnetic field at the cathode, $T_{\perp 0}$ is the cathode temperature that is about 900 °C (100 meV), and B is the magnetic field after expansion. The expansion factors $\varepsilon=B_0/B$ used in this experiment were 16.5 (for $B_\parallel=180$ mT) and 25 (for $B_\parallel=30$ mT). The corresponding electron beam diameters are 1.6 cm and 2 cm, respectively and are given by $R_b=R_{\mathrm{cath}}\sqrt{\varepsilon}$, where R_b is the radius of the expanded electron beam and R_{cath} the radius of the electron

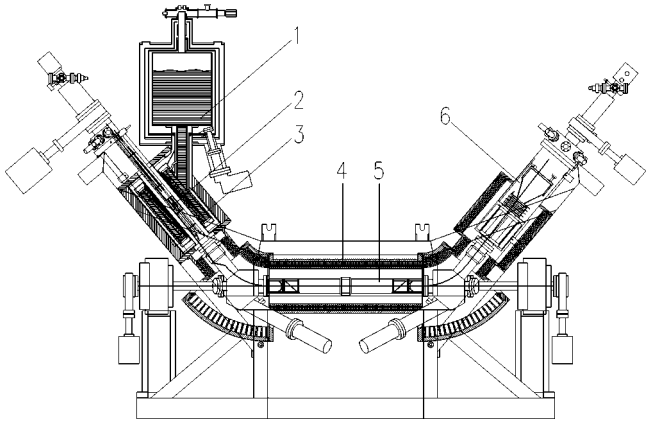

FIG. 1. Schematic of the CRYRING electron cooler with liquid-helium reservoir (1), electron gun (2), superconducting gun solenoid (3), resistive magnets (4), interaction region (5), and electron collector (6).

TABLE II. The initial slope s [see Eq. (12)] as a measure of the electric field enhancement for all DRF measurements carried out so far at storage rings. For Ti^{19+} and Ni^{25+} the average value for the two series $2s\rightarrow 2p_{1/2}$ and $2s\rightarrow 2p_{3/2}$ is given. For each measurement the ion energy E_{ion}, the longitudinal magnetic guiding field $B_\parallel$, and the corresponding cutoff quantum number n_c are given.

Element	$s(10^{-3}$ cm/V)	E_{ion} (MeV/u)	$B_\parallel$ (mT)	n_c
Ne^{7+}	4.4	11.4	30	28
Si^{11+} [a]	10.3	10	30	47
Cl^{14+} [b]	7.45	7.1	30	79
Ti^{19+} [c]	8	4.6	30	115
Ni^{25+} [d]	1.26	5.9	40	150

[a]Reference [5].
[b]Reference [6].
[c]Reference [7].
[d]Reference [8].

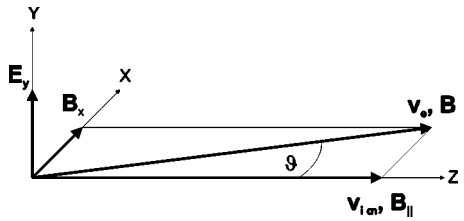

FIG. 2. Sketch of the electric and magnetic field configuration used in DRF measurements. The ion beam is aligned along $B_\parallel$. The motional electric field is $E_y = E_\perp = v_{\rm ion} B_\perp = v_{\rm ion} B_x$ with the ion velocity $v_{\rm ion}$ in z direction. The electron beam with the average velocity v_e is aligned along the resulting B vector that is inclined by the angle ϑ with respect to $B_\parallel$.

beam at the cathode. The transverse energy spread of the electrons obtained by using Eq. (3) is 6.1 meV and 4 meV, respectively. In the interaction region the magnetically confined *cold* electron beam overlaps with the ion beam. The electron density is about 10^7 cm^{-3}. The energy resolution of the experiment is given by the energy spread of the electron beam. The alignment of the ion beam with the electron beam was optimized using correction coils placed on the solenoids. After optimization the ions traveled in the bottom of the electron space-charge well, so there were no transverse fields from space charge and the Lorentz $(\vec{v}\times\vec{B})$ fields in the frame of the ions were minimized. This could be diagnosed by observing the ion beam profile monitor and the Schottky noise frequency spectra of the ion beam. The beam is optimally cooled with perfect alignment, and hence the beam profile in vertical and horizontal directions is minimal. A reasonably *field free* (less then 10 V/cm) measurement of DR could then be obtained by changing the energy of the electrons in the cooler to different values, covering a center-of-mass energy range of $0 < E_{\rm cm} < 20$ eV, corresponding to cathode voltages $6379 < U_{\rm cath} < 7115$ V. Behind the first bending magnet the recombined ions were separated from the primary beam and detected with a surface-barrier detector. The detection efficiency is taken to be 100%.

In order to study field effects, external motional electric fields $(\vec{E}=\vec{v}\times\vec{B})$ were then introduced in the cooler by applying a defined transverse magnetic field $B_\perp$ using the steering coils of the cooler (Fig. 2). Within the experimental uncertainties the measurement is independent of the azimuthal angle ϕ [8]. The magnetic field $B_\perp$ tilts the electron beam while the ion beam is not tilted noticeably. The angle between the beams is given by the ratio of the transverse magnetic field $B_\perp$ and the longitudinal guiding field $B_\parallel$,

$$\vartheta = \arctan\frac{B_\perp}{B_\parallel}. \tag{4}$$

The tilting angle must not be too high, since the beams would not fully overlap anymore. The maximum angle is given by $\vartheta_{\rm max} = \arctan(d_e - d_i)/L$, where d_e is the electron-beam diameter, d_i the ion-beam diameter, and L the interaction length. In order to achieve high transverse magnetic fields at small tilting angles high longitudinal magnetic fields have to be applied. The superconducting magnet at the cathode of the electron cooler allows one to apply these high magnetic fields even at a high expansion of the electron beam, which is needed for the reduction of the transverse energy spread. In the present experiment with an expansion factor of 16.5 and a longitudinal magnetic field $B_\parallel = 180$ mT transverse magnetic fields $B_\perp$ up to 3 mT corresponding to 1400 V/cm could be applied with a tilting angle of only 1°. By tilting the electron beam the ion beam travels through an area with varying space charge potential, which decreases the energy resolution. Moreover, since the electric field caused by the space charge only vanishes in the center of the electron beam, tilting of the electron beam leads to an additional electric field that varies along the overlap section. This field varies between 0 V/cm and 60 V/cm at maximum tilting angle. Since it is small compared to the applied electric fields it is only considered for the determination of the error.

For the measurements, ions were injected into the ring, accelerated, and then cooled for 4 s. After that the complete energy range of the resonances with $7 \leqslant n \leqslant \infty$ was scanned by lowering the voltage at the cathode from 7115 V to 6467 V in 1201 steps. This was done for five different settings of the steering coils (corresponding to five different electric fields) in every cycle (28 s). Between the scans the ion beam was cooled for 1 s. The remaining ions were then dumped and the whole cycle started over using the same settings. This was repeated until a satisfactory level of statistical precision had been reached. Then the measurement continued with a new set of five different electric fields until all five sets (25 fields all together) were completed. The data aquisition was run in the list mode i.e., it was triggered by each pulse from the recombination detector and for each event, the time, the bit value for the energy, and the pulse height were recorded. The dead time was 80 μs.

In storage ring experiments, the maximum Rydberg quantum number of resonant states contributing to the detected signal is limited by field stripping. As the recombined ions travel towards the detector, they encounter three regions with different transverse magnetic fields and hence different motional electric fields. These regions are (1) the toroid that guides the electron beam out of overlap (4.1×10^4 V/cm), (2) a dipole magnet (1.2×10^5 V/cm) just behind the cooler that corrects for the ion beam displacement by the toroidal fields in the cooler, and (3) the bending dipole magnet in which the detector is placed and which is used as the analyzing magnet (5×10^5 V/cm). These fields ionize Rydberg states with quantum numbers n higher than some cutoff value that can be expressed as

$$n_F = (Z^3/9F)^{1/4}, \tag{5}$$

where F is the electric field in atomic units (1 a.u$=5.142\times10^9$ V/cm) [10]. Thus, only recombined ions with $n < n_F$ would reach the detector. This simple formula does not consider radiative decay of Rydberg states on the way to the different field ionization zones, so that the formula for n_F is only indicative. Considering radiative decay of states $n > n_F$ to states below n_F, the cutoff quantum number for this experiment is given by $n_c = 28$ following a hydrogenic ap-

TABLE III. The motional electric fields F leading to field ionization are given for the different magnets through which the recombined ions pass on their way to the detector. The flight time t_F measured from the center of the cooler to the onset of the corresponding field. Δt_F denotes the dwell time in this field. n_F is the critical quantum number for field ionization calculated from Eq. (5).

Region	F (kV/cm)	Δt_F (ns)	t_F (ns)	n_F
Toroid	42	8.2	17	46
Correction magnet	120	4.4	29	35
Dipole magnet	550	25	39	24

proximation for the decay probabilities [11]. In a more detailed field-ionization model we have considered all three field-ionization regions mentioned above to obtain nl-dependent Rydberg detection probabilities denoted by $\Upsilon_{nl}^{(t)}$, $\Upsilon_{nl}^{(c)}$, and $\Upsilon_{nl}^{(d)}$, respectively. The overall detection probability is given by the product of the three individual ones, i.e.,

$$\Upsilon_{nl}=\Upsilon_{nl}^{(t)}(t_F^t,\Delta t_F^{(t)},F^{(t)})\Upsilon_{nl}^{(c)}(t_F^c-t_F^t,\Delta t_F^{(c)},F^{(c)}) \times\Upsilon_{nl}^{(d)}(t_F^d-t_F^c,\Delta t_F^{(d)},F^{(d)}) \quad (6)$$

with t_F denoting the flight time from the cooler center to the entrance of the field ionization zone where the ion spends the time Δt_F. Numerical values used for t_F, Δt_F, and F are shown in Table. III. A detailed description of the field ionization model can be found in Ref. [12]. Figure 3 shows a contour plot of the Υ_{nl}. For $n=26$ the detection probability has decreased to $\Upsilon_{nl}=0.5$ for $l>7$. However lower l states and especially p states contribute significantly to the measured DR rate also at much higher n. Due to the very short lifetimes of these states most of them decay to $n<n_F$ before reaching the field-ionization zone.

III. RESULTS AND DISCUSSION

Figure 4 shows DR spectra of Ne^{7+} ions for five selected electric fields. The spectra show the $2p_{1/2}$ and $2p_{3/2}$ Rydberg series that could only be resolved for small values of n. The

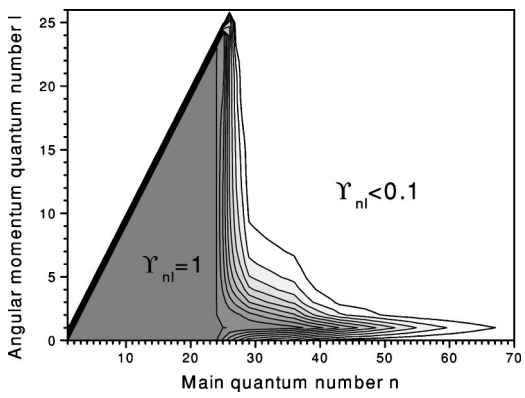

FIG. 3. Contour plot of detection probabilities Υ_{nl} from the detailed model described in Sec. II. A considerable fraction of low-l Rydberg states is detected with high probability even for high n.

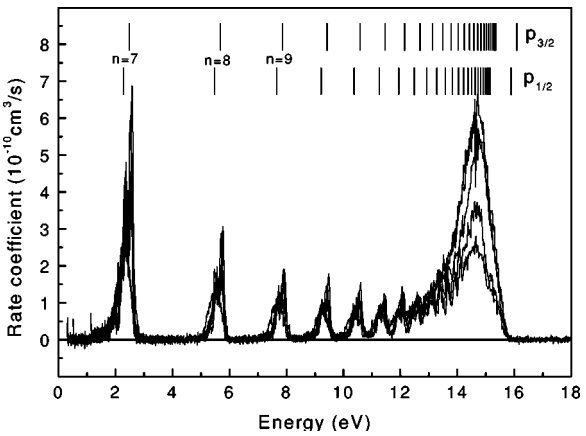

FIG. 4. Ne^{7+} DR spectra for 5 different electric fields 0, 144, 479, 1077, 1316 V/cm. The magnetic field was $B_{\parallel}=180$ mT. The DR rate coefficient for high-n states increases with increasing electric field.

theoretical value for the series limit for the $2p_{1/2}$ ($2p_{3/2}$) transition is 15.8888 eV (16.0936 eV) [13]. The c.m. energy was calculated using a relativistic formula including the angle between the beams (0°–1°). Because of the rather high density of the electron beam ($n_e\approx 10^7$ cm^{-3}) the electron energy T_e in the laboratory frame had to be space charge corrected first:

$$T_e=eU_e=eU_{\rm cath}-eU_{\rm sc}(U_{\rm cath}), \quad (7)$$

where e is the elementary charge and $U_{\rm cath}$ is the voltage at the cathode as applied by the power supply. Possible contact potentials are so small compared to $U_{\rm cath}$, that these are within the uncertainty of U_e. Each $U_{\rm cath}$ is written to the data file. $U_{\rm sc}$ is the potential of the space charge that is calculated using

$$U_{\rm sc}(U_{\rm cath})=\frac{1}{4\pi\epsilon_0 c}\left(1+2\ln\frac{R_D}{R_b}\right)\frac{I_e}{\beta_e}. \quad (8)$$

Here R_D is the diameter of the vacuum tube that is on ground potential. This equation is only valid in the center of the electron beam and has to be solved iterativly since its right-hand side still depends on $U_{\rm cath}$ itself via $\beta_e=v_e/c$. The space-charge potential is around 45 V. The rate coefficient is given by

$$\alpha=\langle v\sigma(v)\rangle=\frac{Rv_iqe}{I_iLn_e}\gamma_i^2. \quad (9)$$

Here R is the counting rate of recombined ions, v_i the ion velocity, q the ion charge state, e the elementary charge, γ_i the Lorentz factor for the ions, I_i the ion current, L the interaction length (0.95 m), and n_e the electron density that can be assumed to be constant across the diameter of the electron beam. In Fig. 4 the background is already subtracted (here radiative recombination is regarded as background) using a formula with 5 fit parameters P_i:

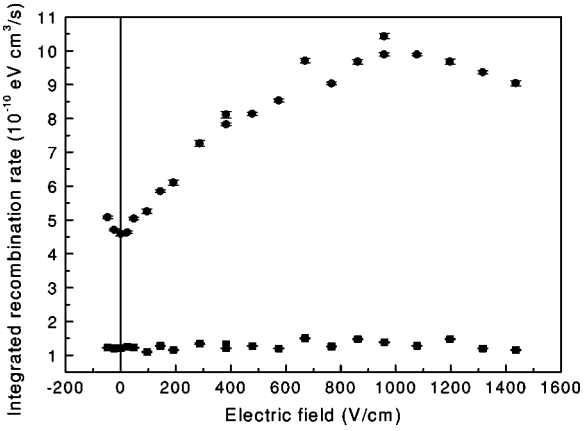

FIG. 5. Integrated recombination rate for the measurement at 180 mT. The circles represent the integrals $I_{\rm hi}$ over energies 11.65–15.9 eV and the squares the integrals $I_{\rm lo}$ over energies 4.5–8.5 eV.

$$\alpha_b(E_{\rm cm}) = \frac{P_1}{1+P_2E_{\rm cm}+P_3E_{\rm cm}^2} + P_4 + P_5E_{\rm cm} \qquad (10)$$

This was fitted to the spectra in energy regions where no DR resonances were present. To keep the rate of electron capture from the residual gas at a low level, high ion energies are needed. At 11.4 MeV/u the signal to noise ratio for the largest DR resonance was about 12:1. For a longitudinal magnetic field $B_\parallel$ of 180 mT the electric field was varied between 0 and 1436 V/cm in 25 different steps. For a second set of measurements the longitudinal magnetic field was set to 30 mT and the electric field was varied between 0 and 144 V/cm in 15 different steps. Absolute calibration was achieved by normalization to data of Zong *et al.* [14]. This was done by comparing the integrated recombination rate for those parts of the *field-free* ($B_\perp = 0$) spectra that are not effected by field ionization. The relative ion currents (for spectra with $B_\perp \neq 0$) were inferred from the recombination rate at cooling, and this was used to calibrate the spectra with respect to each other. The uncertainty for absolute rate coefficients is given by the uncertainty for the ion current measurement ($\approx 10\%$) and for the determination of the interaction length ($\approx 10\%$). The root-mean-square error amounts to 14% [14]. The uncertainties between rate coefficients at different fields are mainly given by uncertainties in determination of the relative ion currents and are about 8%. The statistical uncertainty is below 1%. The uncertainty of the determination of the electric field is mainly given by the uncertainty in electric fields due to the space charge (0–60 V/cm).

The enhancement of the DR via high Rydberg states is quantified by extracting rate coefficients $I_{\rm hi}$ integrated over the energy range 11.65–15.9 eV of the measured spectra covering Rydberg states with n between 13 and 28. For normalization purposes we also monitored the integral $I_{\rm lo}$ (4.5–8.5 eV) comprising contributions to DR from $n = 8-9$. The high Rydberg contributions $I_{\rm hi}$ monotonically increase with the electric field, while the lower n contribution $I_{\rm lo}$ remains constant when the electric field is changed. These integrals are shown in Fig. 5. For very high electric fields one observes a slight decrease of the integrals. This indicates that the electron and ion beams do not fully overlap anymore. In order to provide a quantity characterizing the field effects we use the electric-field enhancement factor [7,8]

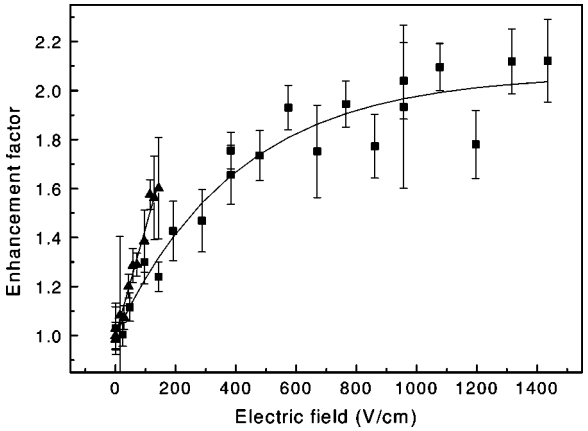

FIG. 6. Electric field enhancement factors for Ne^{7+} ions for two different longitudinal magnetic fields, 180 mT (squares) and 30 mT (triangles). The error bars represent the uncertainty in the relative ion current calibration and the statistical error. The full lines are fits of Eq. (12) to the experimental data.

$$r(E_y, B_\parallel) = C(B_\parallel)\frac{I_{\rm hi}(E_y, B_\parallel)}{I_{\rm lo}(E_y, B_\parallel)}. \qquad (11)$$

The constant $C(B_\parallel)$ has been chosen such that fits to the data points (see below) yield $r^{(\rm fit)}(0, B_\parallel) = 1.0$. The result for the Ne^{7+} experiment is shown in Fig. 6. The formula

$$r^{(\rm fit)}(E_y, B_\parallel) = 1 + s(B_\parallel)E_{\rm sat}(B_\parallel)\left\{1 - \exp\left[\frac{-E_y}{E_{\rm sat}(B_\parallel)}\right]\right\}, \qquad (12)$$

that we have fitted to the measured enhancement factors, provides an easy parametrization of our data. The parameter $E_{\rm sat}(B_\parallel)$ is the saturation field and $s(B_\parallel)$ is the initial slope that is the tangent to $r^{(\rm fit)}(E_y, B_\parallel)$ at $E_y = 0$ (see Table IV). The enhancement factor first grows linearly and then saturates for high electric fields. For these high fields the maximum mixture of l states is achieved. This saturation was already indicated by other measurements [6] but was not seen previously as clearly as in this experiment.

For the smaller longitudinal magnetic field of 30 mT we could not apply as high transverse magnetic fields $B_\perp$ as for 180 mT. The reason for this limitation is the tilt angle ϑ

TABLE IV. Parameters of the fit [Eq. (12)] to the measured data of the enhancement factor for a longitudinal magnetic field of 180 mT and 30 mT. s is the initial slope and $E_{\rm sat}$ is the saturation field. For $B_\parallel = 30$ mT no onset of saturation has been observed.

$B_\parallel$ (mT)	s (cm/V)	$E_{\rm sat}$ (V/cm)
180	2.63+/−0.65	405+/−84
30	4.44+/−0.87	

between the electron and ion beams. The initial slope of the enhancement factor for the measurements at 30 mT is much higher than the slope at $B_{\|}=180$ mT, i.e., the magnetic field reduces the effect of the perpendicular electric field on DR. This confirms previous experimental findings for Cl^{14+} [6] and Ti^{19+} [7] ions.

Compared to other measurements where the detected enhancement of the recombination rate due to an electric field increased from Ni^{25+} ($Z=28$) to Si^{11+} ($Z=14$) (for which the initial slope s_j given in Table II is a measure) the enhancement of the detected recombination rate decreased in the present experiment. This is caused by field ionization of high Rydberg states as has been mentioned in Sec. II. To demonstrate the magnitude of this effect a model calculation of a Ne^{7+} DR spectrum was carried out. Using Eq. (2) a model spectrum is fitted to a measured *field-free* DR spectrum. No quantum defects were considered, i.e., the usual Rydberg formula

$$E_n = E_\infty - \mathcal{R}\left(\frac{q}{n}\right)^2 \tag{13}$$

has been used, with the Rydberg constant $\mathcal{R}$, the ion charge q, and the series limit E_∞. For the radiative rates A_r values obtained by the Cowan atomic structure program [15] were used. The autoionization rates A_a were modeled following reference [3],

$$A_a(n,l) = A_a^{(0)}(1/n^3)\exp(-l^2 d). \tag{14}$$

$A_a^{(0)}$ and d are obtained by the fit to the experimental spectrum. All model parameters are given in Table I. Since the $1/n^3$ dependence for A_a is only valid for high n states values below $n=10$ were not included in the fitting. The resonances occurring above 14.5 eV were not included in the fit either, because field ionization becomes already noticeable in this region of the DR spectrum. Once a good fit is obtained all parameters except the maximum quantum number n_c are set constant. For $n_c>100$ the total recombination rate does not increase significantly anymore. Figure 7 shows the results for the complete extrapolated DR spectrum.

To this spectrum, the field-ionization model has been applied calculating nl-dependent detection probabilities Υ_{nl} as described in Sec. II. The result is shown in Fig. 7 and very closely reproduces the experimental data. From this we conclude that field ionization in our experiments is sufficiently well understood.

A proper estimation of the unmeasured rate enhancement in principle requires a full theoretical treatment of the Ne^{7+} DR in crossed electric and magnetic fields. Such a calculation is presently not at hand and certainly beyond the scope of this work. In this situation we can only obtain a rough estimate of the unmeasured field effect by refering to a DRF theory for O^{5+} [16] an ion that is reasonably close in nuclear charge to Ne^{7+}. In the O^{5+} theory the maximum enhancement is found to be $\sigma^{DRF}(n)/\sigma^{DR}(n)\approx 6$ at $n\approx 50$. In a recent experiment with O^{5+} ions [17] the measured enhancement amounts to a factor of 2. This is considerably lower than the theoretical result because of two reasons. (i) Individual n resonances have not been resolved. The measured enhancement, therefore, represents a mean value averaged over a range of Rydberg resonances. Over this range the theoretical ratios $\sigma^{DRF}(n)/\sigma^{DR}(n)$ exhibit a strong variation. (ii) The field-ionization-cutoff value has been at $n_c=25$ only with $\sigma^{DRF}(n)/\sigma^{DR}(n)$ being 3.6 only. On the basis of the theoretical O^{5+} result we estimate that extending the range of n values to $n=100$ would increase the measured enhancement roughly by a factor of 2. A similar value for the unmeasured field-induced rate enhancement can be expected to hold for the present experiment also.

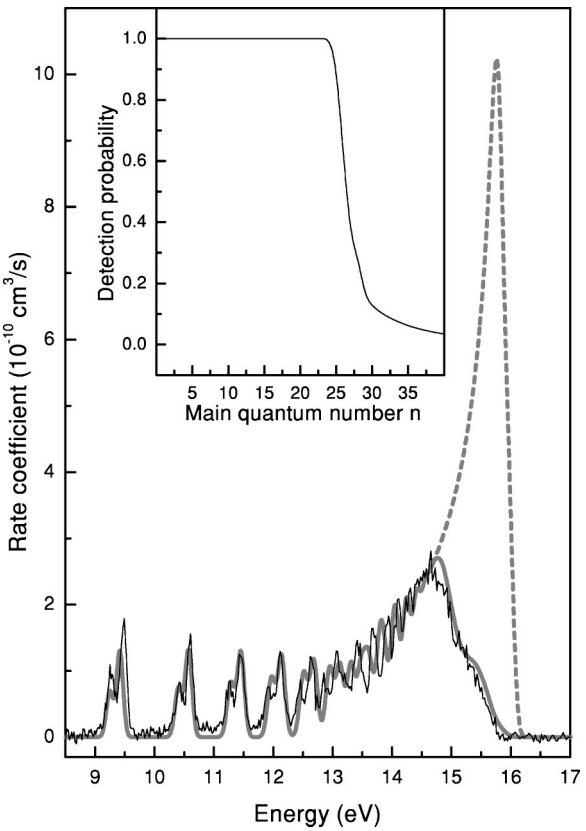

FIG. 7. Measured "field-free" Ne^{7+} DR spectrum and outcome of the model calculation with $n_c=100$ (dashed line). When field ionization in the charge state analyzing dipole magnet is accounted for the model calculation results in the full gray line. It very closely reproduces the measured spectrum. The inset displays l-averaged detection probabilities $\overline{\Upsilon}_n = n^{-2}\Sigma_l(2l+1)\Upsilon_{nl}$ derived from the Υ_{nl} shown in Fig. 3. It suggests that for a meaningful comparison with the experimental data theory has to include states up to at least $n=30$.

IV. SUMMARY AND CONCLUSIONS

The influence of electromagnetic fields on DR could clearly be seen in this experiment. The recombination rate at 14.5 eV, i.e., near the series limits of Rydberg resonances, increased by a factor of up to 2 compared to the field-free case. The enhancement first grows linearly and then saturates for high electric fields. A clear dependence on the strength of the magnetic field perpendicular to the electric field (in this case $B_{\|}$) was observed as in the experiments with Cl^{14+} and

Ti^{19+} ions. The initial slope of the enhancement factor versus electric field was increased almost by a factor of 2 by lowering $B_{\|}$ from 180 mT to 30 mT. The expected larger enhancement due to a lower Z could not be detected because field ionization begins at lower fields than in other experiments of this series on Li-like ions. This has been demonstrated by a model calculation for the field-free spectrum. For a thorough understanding of the observed field effects a comparison with DRF theory including both electric and magnetic fields is vitally needed. Because of the absence of any spatial symmetry such a theory requires the explicit treatment of all m substates in the diagonalization procedure. Computer-storage constraints currently prevent such calculations from being carried out for very high Rydberg quantum numbers. The highest value considered so far has been $n=24$ [18]. Our field ionization model shows that a meaningful comparison with the present experimental data requires a calculation up to at least $n=30$ (inset of Fig. 7). In view of the continuing progress of computer technology we are confident that such a calculation will become feasible in the near future.

ACKNOWLEDGMENTS

We gratefully acknowledge support by the Bundesministerium für Bildung und Forschung (BMBF), Deutsche Forschungsgemeinschaft, and the Office of Fusion Energy Sciences of the U.S. DOE through Contract No. DE-A102-95-Eh54993 with the National Institute of Standards and Technology.

[1] A. Burgess and H.P. Summers, Astrophys. J. **157**, 1007 (1969).
[2] H. Bachau, R. Gayet, P. Lambropoulos, P. Schlagheck, and A. Wolf, J. Phys. B **31**, 3263 (1998).
[3] A. Müller, D.S. Belić, B.D. DePaola, N. Djurić, G.H. Dunn, D.W. Mueller, and C. Timmer, Phys. Rev. A **36**, 599 (1987).
[4] D.C. Griffin, F. Robicheaux, and M.S. Pindzola, Phys. Rev. A **57**, 2708 (1998).
[5] T. Bartsch, A. Müller, W. Spies, J. Linkemann, H. Danared, D.R. DeWitt, H. Gao, W. Zong, R. Schuch, A. Wolf, G.H. Dunn, M.S. Pindzola, and D.C. Griffin, Phys. Rev. Lett. **79**, 2233 (1997).
[6] T. Bartsch, S. Schippers, A. Müller, C. Brandau, G. Gwinner, A.A. Saghiri, M. Beutelspacher, M. Grieser, D. Schwalm, A. Wolf, H. Danared, and G.H. Dunn, Phys. Rev. Lett. **82**, 3779 (1999).
[7] T. Bartsch, S. Schippers, M. Beutelspacher, S. Böhm, M. Grieser, G. Gwinner, A.A. Saghiri, G. Saathoff, R. Schuch, D. Schwalm, A. Wolf, and A. Müller, J. Phys. B **33**, L453 (2000).
[8] S. Schippers, T. Bartsch, C. Brandau, A. Müller, G. Gwinner, G. Wissler, M. Beutelspacher, M. Grieser, A. Wolf, and R.A. Phaneuf, Phys. Rev. A **62**, 022708 (2000).
[9] H. Danared, G. Andler, L. Bagge, C.J. Herrlander, J. Hilke, J. Jeansson, A. Källberg, A. Nilsson, A. Paál, K.-G. Rensfelt, U. Rosengård, J. Starker, and M. af Ugglas, Phys. Rev. Lett. **72**, 3775 (1994).
[10] T.F. Gallagher, *Rydberg Atoms* (Cambridge University Press, Cambridge, 1994).
[11] A. Müller and A. Wolf, Hyperfine Interact. **107**, 233 (1997).
[12] S. Schippers, G. Gwinner, J. Linkemann, A. A. Saghiri, A. Wolf, and A. Müller, Astrophys. J. **555** (2001).
[13] Y.-K. Kim, D.H. Baik, P. Indelicato, and J.P. Desclaux, Phys. Rev. A **44**, 148 (1991).
[14] W. Zong, R. Schuch, H. Gao, D.R. DeWitt and N.R. Badnell, J. Phys. B **31**, 3729 (1998).
[15] R.D. Cowan, *The Theory of Atomic Structure and Spectra* (California University Press, Berkeley, 1981).
[16] D.C. Griffin, M.S. Pindzola, and C. Bottcher, Phys. Rev. A **33**, 3124 (1986).
[17] S. Böhm, S. Schippers, W. Shi, A. Müller N. Djurić, G.H. Dunn, W. Zong, B. Jelencović, N. Eklöw, P. Glans, R. Schuch, H. Danared, and N.R. Badnell, Phys. Scr. **T92**, 395 (2001).
[18] D.C. Griffin, F. Robicheaux, and M.S. Pindzola, Phys. Rev. A **57**, 2708 (1998).